Testing to Establish Main Steam Line Standing Wave Patterns and Relationships to Side Branch Resonance

University of Tennessee, Department of Nuclear Engineering

Authors: Arthur E. Ruggles PI (aruggles@utk.edu)
Brian Wood
Eric Moore

Prepared for the TVA under release #72 2007-RUGGLES

Abstract: Experiments have been conducted at the University of Tennessee Department of Nuclear Engineering to promote understanding of the relationship between side branch acoustic resonance and standing waves in the main lines of nuclear steam supplies. Experiments to date have exposed drift in side branch resonance frequency with position relative to the standing wave pattern in the main line. Experiments are underway to examine interaction between branches that may be important to planned modifications to the Browns Ferry Units, and to simulate branches similar to dead legs found on the Browns Ferry units. This report documents facility development and experimental activities from August to December, 2007.

Table of Contents

Introduction and Background:

The Browns Ferry Nuclear Power Station Units 1, 2 and 3 seek extended power uprates equal to 120% of original licensed thermal power (OLTP). The power increases are accomplished through increase in the steam flow from the reactor core. Other power uprates in the BWR fleet resulted in excitation of ¼ wavelength standing waves in the side branches used for safety relief valves (SRV). These resonances excited standing waves in the main steam lines that loaded components in the steam supply. The steam dryer assembly in a Quad Cities unit was damaged by these acoustic loadings.

Browns Ferry Units have nine safety relief valves in the flow on the main lines with resonance frequency near 112 Hz. The Browns Ferry Units also have eight so-called blind flange branch lines with resonance frequency near 220 Hz.

Main line acoustic pressure measurements have been used to predict steam dryer loading and steam dryer stress. Those predictions indicated the narrow band resonance of the blind flange branches found in the main line signal will fatigue the dryer. TVA proposed to plug those branches so that the cavity for acoustic resonance is removed.

The side branch resonance is driven by vortices shed across the branch opening. These vortices couple with the acoustic displacements at the branch opening so that a range of flow velocities can excite a branch resonance. Usually the Strouhal number, fD/v, corresponding to resonance is between 0.3 and 0.55, with peak amplitudes occurring between 0.4 and 0.5. Where f is frequency, D is the branch diameter and v is the flow velocity in the main line. However, a second mode can exist for Strouhal numbers from 0.8 to unity. The blind flanges are excited by the second mode of vortex shedding. The SRV branches are of the same diameter and thus fall in the range of Strouhal numbers where excitation is expected by the first mode of vortex shedding. However, no significant indication of SRV branch resonance exists in the plant data.

Branches can communicate through the main line, as first examined by Bruggeman, 1987, 1991, and the branch resonance frequency is influenced by the standing wave pattern in the main line as reported by McKinnis et al, 2007. These data indicate the vortex shedding can be influenced by the standing waves in the main line, as well as by the acoustic displacements in the branch. The aero-acoustic theory also supports such relationships. However, the theories and the data are incomplete, and definitive predictions are not possible.

An experiment was proposed, building on past explorations published by McKinnis, 2007, that would examine if the high frequency standing wave pattern created by the blind flange branches could be suppressing an expected resonance in the lower frequency SRV banches. The SRV resonance was not observed in the plant data at current licensed thermal power (CLTP), but was observed at scaled CLTP in tests performed by GE for TVA. Interestingly, the GE scaled tests also did not show the high frequency blind flange resonance that is observed in the plant data. The GE test was at 1/17 scale, so the second vortex shedding mode at Strouhal equal 0.8 to unity may not be possible, so the blind flanges were not excited. So the hypothesis that the high frequency standing wave may suppress the lower frequency resonance in the SRV branch of the same diameter fits past data anomalies.

The facility at UT is low pressure and 1/8 scale (3 inch diameter main line, ¾ inch and 1 ½ inch branch lines), so the second mode of vortex shedding may still not be possible. Therefore, the high frequency standing wave is produced with a ¾ inch diameter branch of length near 6 inches, and the lower frequency branch is of diameter 1 ½ inches, and near one foot long. The branches were initially constructed with adjustable plugs, following an example used by other researchers. The facility can achieve Mach number equal 0.14 using air at one atmosphere.

Initial testing using the two adjustable branches yielded unusual data, especially with respect to the range of velocities for which resonance could be achieved for the small branch. However, several branch lengths and several branch positions were tested, with the small branch in resonance. In a few cases we could alter the small branch resonance (turn it on and off) by adjusting the large branch cavity length.

The unusual values of Strouhal number corresponding to resonance for the short branch motivated some additional instrumentation, including a second flow measurement device, and additional microphones capable of higher amplitude measurements. With the new instruments in place, a series of more simple tests with the individual branches were initiated. The small branch resonance peak is occurring near Strouhal number 0.3 when standing waves are allowed to set up in the main line. This is well below the expected values for the peak of 0.4 to 0.5. These discoveries led to need for more ease of flow velocity control, so a 3 inch ball valve was positioned on a bypass to allow ease of flow velocity variation. Concern about this result also led to experimental comparison of the adjustable branch design with the previously used capped branch design. These comparisons are underway.

With the behavior of our individual components characterized, we plan to return to multiple branch testing with the additional instrumentation to thoroughly examine the influence of the small branch on the larger branch. There are several parameters that must be varied to conduct a thorough test. For a given small branch position, the relative position of the large branch to the small branch must be varied, allowing the large branch to experience various parts of the standing wave pattern in the main line. For each relative position the flow velocity must be varied so a range of Strouhal numbers is encountered from 0.2 to 0.6. Data from the three microphones and two flow meters are collected for each condition.

There is some possibility that the position of the small branch relative to the ends of the main line has some effect, so two or three small branch positions will be tested, following the entire sequence of data collection previously described. This campaign should conclusively establish if or when the small branch high frequency resonance can influence the longer lower frequency branch behavior.

Additional to these tests a simulation of the dead leg resonance is planned to duplicate the flow across the dead leg "branch" and examine when vortex shedding can excite resonance in that configuration. A small six inch branch design with a cross-sectional area change, similar to that in the SRV branch, has been fabricated for testing to see if this design detail influences the branch acoustic behavior, and helps to explain current conundrums in the existing scale model and plant data.

The report that follows explains the facility we have developed and catalogues some of the testing underway. The total TVA investment in testing to date, including previous testing conducted by McKinnis in 2006, is near $23,000. This includes student hourly time at $10.00/hr, instrumentation, data acquisition, and materials. The remainder of the total project costs, which includes due diligence review activities and several technical evaluations, cover my time and travel. Work from 2006 is covered in the McKinnis paper from May, 2007, which is provided at the end of the Reference section of this report.

Experimental Facility:
A 3.7 kW Dayton™ model 3N669A blower was used to draw air through the testing facility's 3 inch main line. The blower was placed outside the building to help reduce to noise it created from interfering with the testing microphones. It was connected to the flow control mechanism by flexible aluminum tubing. The main line rested under a folding work table on the table's legs. Several layers of bubble wrap separated the main line from contact with the table, which provided vibration isolation from outside sources that contacted the table. A typical example of the testing facility configuration can be seen in Figure 1.

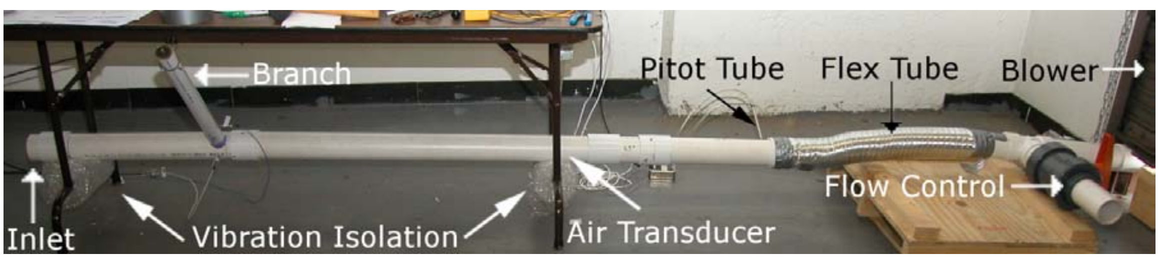

Figure 1: General Test Facility Setup.

The flow was controlled by a 3 inch ball valve, as seen in Figure 2. It was placed on a "T" off of the main line in order to reduce to the amount of noise created from the ball valve. Flow in the main line is reduced by allowing additional inlet bleed flow through the ball valve branch.

Figure 2: Flow velocity control device, PVC 3 inch ball valve.

Directly upstream from the ball valve intersection another piece of flexible aluminum tubing was used to connect to the main line so that any noise coming from the blower or ball valve can escape through the flexible tubing. The main line length is variable around a nominal 8 foot value, and 3 inches in diameter made of schedule 40 PVC. At the end of the main line, directly upstream of the perforated aluminum tubing, a 16 5/8 inch piece of PVC contained the Pitot tube. Capped and adjustable plug branches, shown in Figure 3 and Figure 4 of ¾ inch in diameter and 1½ inch in diameter respectively, were examined.

Figure 3: Capped Branch

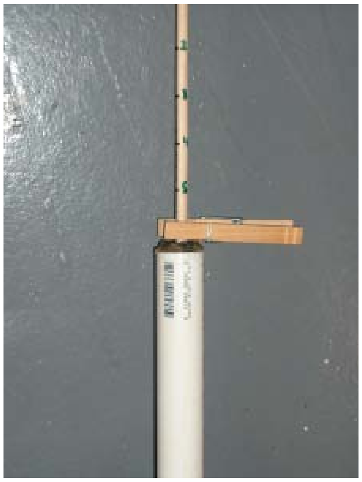

Figure 4: Adjustable Branch

The cap was made of schedule 40 PVC with a rounded inside and the ¾ inch and 1½ inch capped branches were 6 inches and 18 inches respectively in length. The adjustable branches were constructed exactly the same as the capped branches, except for the ability to change the branch length for the adjustable branch. A solid PVC plug was tightly fitted to the inner diameter of the branch using a lathe. The plug had a flat bottom surface forming a flat inner surface in the branch opposed to the capped branch that had a curved inner top surface. The ¾ inch adjustable branch had 12 inches of active possible length and the 1½ inch adjustable branch had 18 inches. The branches were placed directly in a 24 inch piece of the main line 2 inches from the edge of the spool piece. The branch to main line junction shown in Figure 5 was constructed with sharp edges at right angles to the main line.

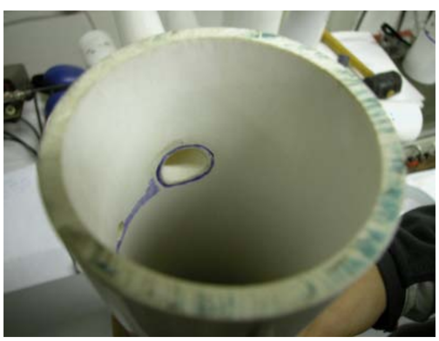

Figure 5: Branch to Main Line Sharp Junction

The influence of the branch position in the main line was investigated by testing each branch in the main line at distances of 24, 42, and 48 inches from the inlet. Various lengths of PVC piping were used to change the distance from the inlet for each branch test, while keeping the main line length constant at 8 feet for these tests. The distances of 24 inches and 48 inches were chosen because they are equal to an integer number of wavelengths of the main line standing wave, whereas the distance of 42 inches was not and provided a complete look at how the position of the branch in the main line influences the resonance frequency in the branch.

In order to keep track of all the degrees of freedom involved in this investigation a test matrix was developed. The matrix allowed inputs for each test: branch length, branch diameter, capped or plugged, branch distance from inlet, resonance frequency, and flow velocity. The test matrix was attached to the data files for that particular experimental setup to allow for more accurate data analysis.

Flow Measurement:

The task of correctly measuring the flow velocity in the main line is vital to this experiment; therefore, two air flow measuring devices were incorporated. A Pitot tube was installed in previous experiments using this facility (McKinnis et al, 2007) and it was used again for the current experiment. The Pitot tube operation in this application is examined in Appendix A. The pressure difference generated by the Pitot tube was sent to an Omega differential pressure transmitter (PX653-05D5V) powered by a high-quality power supply (HP 6253A). The Omega transmitter produced a voltage that was converted into a flow velocity using a MATLAB code given in Appendix B, using the pressure transmitter calibration data provided in Appendix C. The output voltage was then displayed in the data acquisition system comprised of a National Instruments DAQ (NI USB-9162) and LabVIEW 8.0. The signal collected by the data acquisition system had a sinusoidal characteristic an AC ripple which was removed through averaging, but otherwise the instrument functioned as expected. The source of the ripple will be investigated further in later experiments. The data acquisition system recorded 30,000 samples with a delta time of 0.0001 seconds, which resulted in an average displayed every 3 seconds. This provided a steady voltage that was then inserted into the MATLAB code given in Appendix B, which adjusted for pressure and temperature variations and calculated a flow velocity in feet per second. In order to verify the flow detected by the Pitot tube, a second flow velocity measurement device was purchased.

The second flow velocity device used was an air velocity transducer, the Omega FMA-906V. Its specifications and calibration sheet can be found in Appendix D. The air velocity transducer was placed in the main line at a great enough distance upstream from the Pitot tube (about 20 inches) to prevent any flow disruption directly before the Pitot tube. The transducer outputs voltages ranging from 0 to 5 volts which corresponds to a range of velocities of 0 to 10,000 ft/min. Omega's calibration for this instrument provides the initial conversion of voltage in volts to velocity in ft/min, which is then converted to ft/sec for the range of velocities capable in the experimental facility, shown in Figure 1. This air flow measuring device uses a hot film sensor that automatically adjusts for temperature and pressure variations. Figure 6 displays the flow velocity curve used to calculate the velocity from the voltage outputted by the transducer. The voltage produced was averaged and displayed in the data acquisition system in the same way as the Pitot tube's output, which provided a consistent voltage that could be inserted into the transducer's calibration curve, Equation 1, to give a flow velocity in ft/sec.

$$\text{Transducer Flow Velocity (ft/s)} = [(V_{avg} - 0.0221)]/0.03 \quad \textbf{(1)}$$

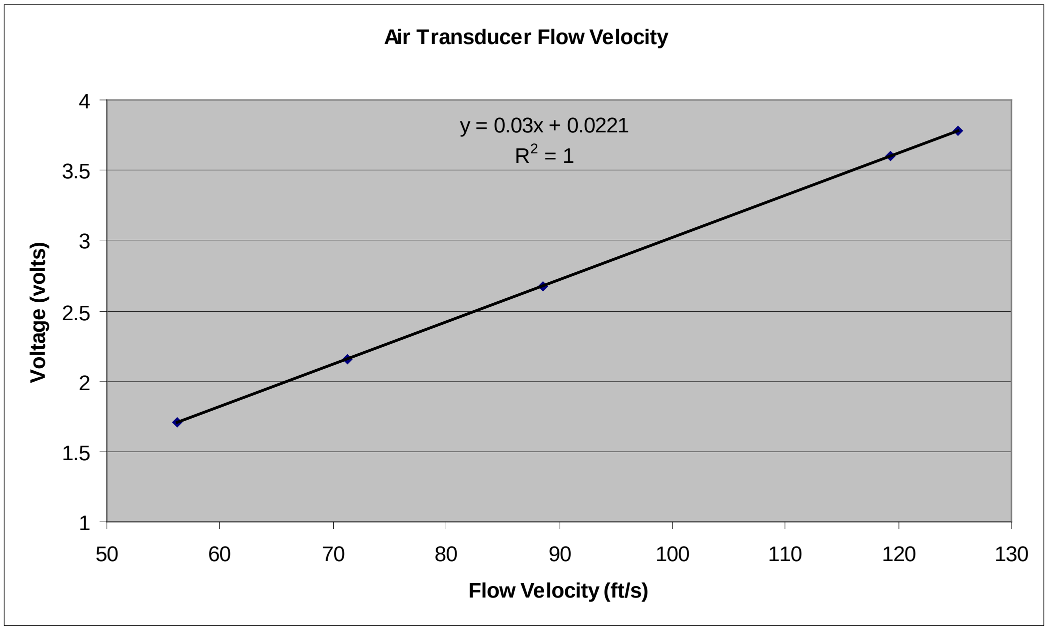

Figure 6: Transducer Flow Velocity Plot

Measurements were taken from both devices for various flow bypass valve positions to provide a range of flow velocities so that any difference in the measured velocities could be seen. A plot of the measured velocities of both devices is shown below in Figure 7.

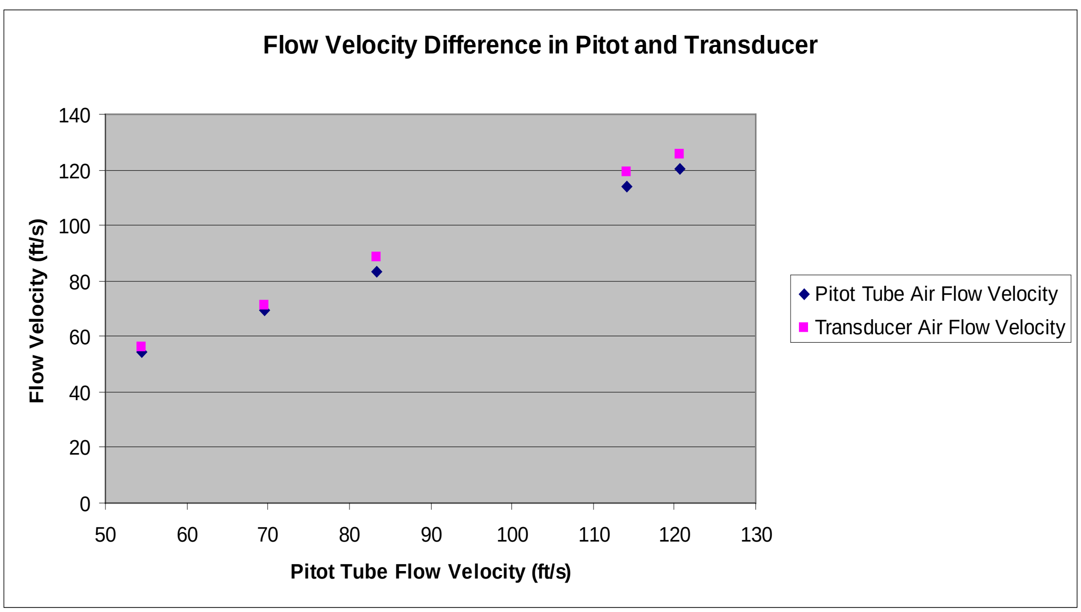

Figure 7: Pitot Tube and Transducer Predicted Flow Velocities

The flow velocity from the transducer was slightly higher than the Pitot tube at various velocities ranging from the minimum to the maximum velocities of the experimental facility. The measurement of the flow velocity to accuracy less than 5% proved to be difficult, therefore Pitot tube theory and corrections were developed to try to discover the reason for the difference, with some of these activities documented in Appendix A.

Acoustic Measurement:
The acoustic measurement system was constituted by a PCB microphone setup which was sampled at 10 kilohertz by a personal computer using LabVIEW. The same National Instruments DAQ (Data Acquisition Unit) used for flow measurement provided analog-to-digital conversion of the amplified microphone signals. The LabVIEW program calculated a Fast Fourier Transform on the signals, yielding frequency amplitudes in the frequency range of 0-5000 hertz. In operation, resonant frequencies were then discovered by noting local maximums in the FFT.

Three PCB microphones were in use, with model numbers 377A12, 377B01, and 377B10. The unit with the lowest maximum pressure (377B010) could handle 165 dB at the 3% distortion limit. The microphone preamplifiers were PCB model number 426B03. The two microphones with integral preamplifiers are illustrated in Figure 8 below. The specification sheets for the microphones and preamplifier can be found in Appendix E.

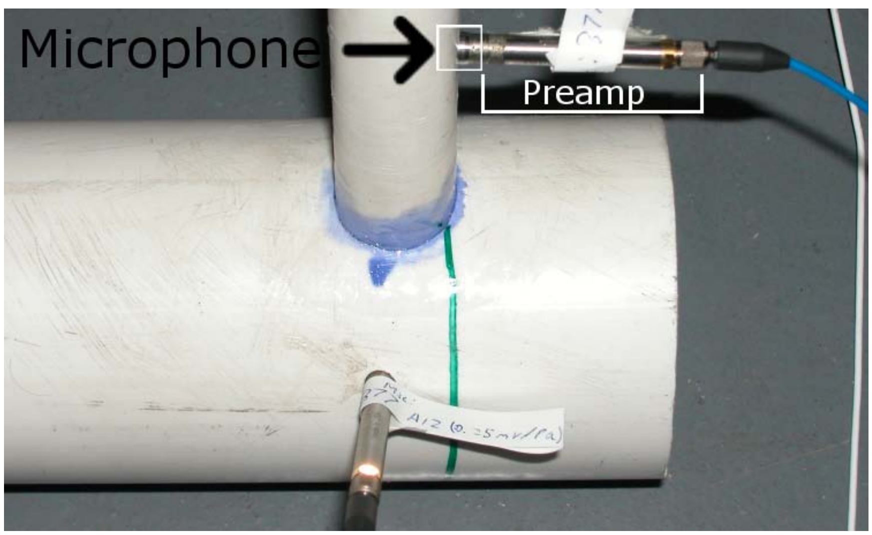

Figure 8: Location of Microphones in Branch and Main Line

The signals were amplified for the DAQ by a PCB model 482A12 run at 1x gain. The DAQ was a four-port NI USB-9162; three of the ports were utilized for acoustic measurement.

The LabVIEW implementation used for acoustic measurement displays and recorded both the raw pressure versus time data and the FFT amplitude versus frequency data. Each test run's raw data was stored on the personal computer along with a commented test matrix file listing the test parameters and frequency maxima encountered. The pressure and FFT data was recorded in tab-delimited format so that experimental data may be used by various software packages.

Conclusions and Work in Progress:

The majority of past experiments studying side branch resonance in the literature used mufflers to absorb sound generated in the main lines. This allowed detailed evaluation of the side branch as an acoustic energy source, but did not lead to characterization of how side branches interact with main line standing wave patterns. The degrees of freedom in the acoustic system are several when a single branch is present, and a standing wave is allowed to set up in the main line, making characterization of the system performance much more challenging, but this has been successfully undertaken in previous work in our facility, disclosing that side branches can resonate over a range of frequencies, depending on the standing wave pattern in the main line. We have also found that the Strouhal number corresponding to resonance can be shifted to lower values than previously reported for situations where standing waves exist in the main lines.

Movement to study of multiple branches positioned on a main line where standing waves are allowed to build, has again escalated testing complexity. Additional instrumentation combined with better understanding of underlying physical behavior has led us to a testing strategy that allows examination of branch interactions when the branches have unequal resonant frequencies. Sound pressure levels in the branch, and in the main line at the branch location are monitored, and a third sound pressure instrument is moved throughout the main line to characterize the pressure field there.

Testing is underway to examination of how design details in a single branch influences the acoustic performance of that branch. Our adjustable branches and fixed length branches are being compared, and a side branch with a shoulder similar to that existing in the SRV branch lines where the valve body attaches to the branch is ready for testing. Those tests will be complete in January. A thorough plan for examination of interaction between branches of unequal length has been developed and is presented herein. Some of those tests are complete, and reporting on outcomes will be completed by February ending. Materials are in place to configure the facility such that it simulates flow past a dead leg.

The various discoveries and associated adjustments and investigations have extended our original schedule for delivering outcomes for the multiple branch tests. However, additional knowledge and understanding of side branch resonance, and how these resonances interact with main line standing waves, has been generated during these efforts. This knowledge is pertinent to the design of steam supply systems and development of performance assessment methods, and much of this information is helpful to TVA efforts to understand and predict acoustic loading of the Steam Dryers in the Browns Ferry Units.

Appendix A: Pitot Tube Theory, Corrections, and Data Acquisition Software

The test facility uses two forms of air flow measurement. The first measurement technique, used in previous tests by McKinnis et al, 2006, is a pitot-static tube (Dwyer model 160-8CF). The Pitot tube has 3/8 inch outside diameter, and is placed near the centerline of the 3 inch diameter main line. The Pitot tube design has the stagnation pressure line concentric to the static pressure line, allowing local velocity measurements without static pressure bias. However, in this application the tube diameter is a significant portion of the total test section cross section, causing the main line flow to accelerate slightly due to the obstruction caused by the Pitot tube. The flow acceleration lowers the static pressure at the location of the static ports on the outer tube diameter. The Pitot tube is shown in the schematic and picture provided in Figure A-1.

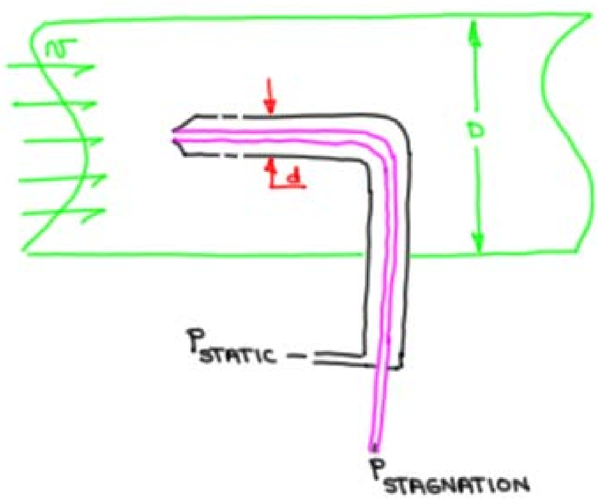

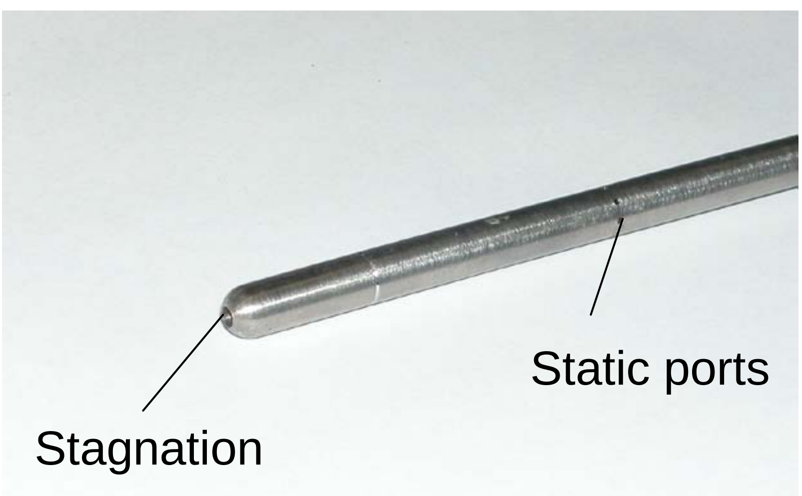

Figure A-1: Pitot Tube Design and Position in Main Line plus Picture of Pitot Nose.

The basic theory of the Pitot tube operation for a horizontal flow is derived from the Bernoulli equation,

$$P + (1/2)\rho v^2 = Const. \tag{A1}$$

Flow streamlines stagnated on the front of the tube convert flow kinetic energy to pressure, the stagnation pressure,

$$p_{stag} = p_{static} + (1/2)\rho v^2 \tag{A2}$$

Normally flow velocity is predicted from the measured difference between the stagnation pressure and the static pressure, such that,

$$v = \left\{ \frac{p_{stag} - p_{static}}{(1/2)\rho} \right\}^{1/2} \tag{A3}$$

The flow moving past the static ports is accelerated due to the reduced cross sectional area in the main line, reducing the static pressure from that in the main line upstream, and this can be evaluated using a mass balance,

$$\rho v_{us} \pi D^2 = \rho v_{pt} \pi [D^2 - d^2] \tag{A4}$$

Where D is the main line diameter and d is the pitot tube diameter. The static pressure will be reduced, causing the pitot tube to over predict the flow velocity in the main line. In our case the pitot tube diameter is 3/8 inches, and the main line diameter is 3 inches, so if density is taken constant,

$$v_{pt} = v_{us} \left[\frac{D^2}{D^2 - d^2} \right] \tag{A5}$$

Such that the velocity is accelerated by a factor of 1.043. This will reduce the static pressure by nearly 8.9 percent. Since the flow pressure differences are attributable to changes in the flow kinetic energy term, and since the pressure variations go as the velocity variations squared, the Pitot tube velocity bias is positive 4.3 percent, and the measured velocity values should be reduced by a factor of 0.959 to account for the flow obstruction caused by the instrument.

Pitot Tube Unit Conversions and Thermo-physical Property Values:

The air density is a function of the temperature and pressure at the Pitot tube location. The air properties are taken from NBS Circular 564, at one atmosphere and 300 Kelvin, and the ideal gas law is used to project properties around that value,

$$\rho = \frac{p}{RT} \tag{A6}$$

The density is well approximated as,

$$\rho = \frac{p}{286.9 * T} \tag{A7}$$

With the pressure in Pa, temperature in degrees Kelvin, and density in Kg/m^3. Pressure varies due to weather are neglected, but the influence of the elevation of Knoxville, and the reduction in pressure due to test section operation near Mach 0.1 are included. Lab data acquisition software asks for temperature information prior to testing.

B: MATLAB Code

```
%10-12-2007 author Eric Moore code for TVA project, Dr Ruggles
%Given ambient temperature and voltage of Pitot tube reading, return
%velocity of air at Pitot tube


Atemp=input('What is the ambient temperature in Celcius?');
%convert to Fahrenheit
Atemp = Atemp*1.8 +32;
resp=input('Voltage to velocity (1) or velocity to voltage (2)');
if resp==1
    Ovoltage=input('What is the Omega voltage reading?');
end
if resp==2
    Ovelocity=input('What is the desired velocity?')
end


%knoxville average elevation = 936 feet, calculate atmospheric pressure
w/
%barometric formula (gives in inches Hg)
Patm=29.92126*(288.15/(288.15+(-
0.0019812)*(936)))^(32.17405*28.9644/(8.9494596*10^4)/-0.0019812);
%density air formula based on absolute static pressure (atm + static in
%tube) and temp, gives in lbm/ft^3, 0.386 inHg = 5in H2O)
%note: changed + to -.368 (on Ruggle's advice)
%note: 1.325 is lbm/ft^3 * rankine per in hg
densityair=1.325*(Patm-0.368)/(Atemp+460)
%density of water formula in kg/m^3

%densitywater = 1000*(1 -
(Atemp+288.9414)/(508929.2*(Atemp+68.12963))*(Atemp-3.9863)^2);
%formula seems to be incorrect, use easy value for n ow
densitywater = 998;

%convert to lbm/ft^3
densitywater = densitywater / 16.0184634

%least squares fit for Omega differential pressure transmitter


Op_cal=[0 1.25 2.5 3.75 5 3.75 2.5 1.25 0];
Ov_cal=[1.005 2.005 3.003 4.001 5.005 4.001 3.005 2.009 1.009];
if resp==1
[Ofit]=polyfit(Ov_cal, Op_cal, 1);
inches=Ofit(1)*Ovoltage+Ofit(2)
if inches<0
    disp('The curve fit is invalid for this voltage (negative inches of
water!)')
end
end


if resp==1
```

```
%pressure = density * gravity * inches(height)
%solve for pressure
pressurefrominches=densitywater * 32.2 * (inches/12);
%pressure=0.5*p_air*v^2
v=sqrt(pressurefrominches*2/densityair)

end

if resp==2
    pressurefrominches=(Ovelocity^2)/2*densityair;
    inches=pressurefrominches*12/densitywater/32.2

      [Ofit]=polyfit(Op_cal,Ov_cal,1);
    polyvolt=Ofit(1)*inches+Ofit(2)

end
```

C: Pitot Tube Differential Pressure Cell Calibration from Omega

CALIBRATION REPORT

Accuracy Class: .5 %
Pressure Range: 0.00 / 5.00 "WC
Output Type: 1 - 5 VDC
Serial Number: 60323043
Date: 03-23-2006

Pressure "WC (Ref 4C)	Output VDC/ma	Error % FSO	Error % BSL
0.000	1.005	0.11	0.00
1.250	2.005	0.12	0.01
2.500	3.003	0.08	-0.04
3.750	4.001	0.02	-0.10
5.000	5.005	0.12	0.01
3.750	4.001	0.02	-0.09
2.500	3.005	0.12	0.01
1.250	2.009	0.22	0.10
0.000	1.009	0.21	0.09

Excitation Voltage: 24VDC
System Number: I

We certify that our calibration system complies with ISO 10012-1, ANSI/NCSL Z540-1 and that all standards used for calibration are traceable to the National Institute of Standards and Technology. Pressure Standards: #215451, & #737/202491-60. Electrical Standards: DC Volts 251625, AC Volts 245061, Res 811/251319, Freq VLF WWVB, Resistor - AC 100072,DC 100071, R 100073 and FWWVBULSREC.

$$\%\ \text{FSO Error} = \frac{\text{Vout} - \left[V_{FS}\ \text{X}\ \dfrac{\text{PRESSURE} - \text{PRESSURE}_{0\%}}{\text{PRESSURE}_{FS}} + \text{Vout}_{0\%} \right]}{V_{FS}}\ \text{X}\ 100$$

$V_{FS} = \text{Vout}_{100\%} - \text{Vout}_{0\%}$ (Theoretical Max and Min)

Reference ANSI/ISA-S51.1 & ANSI/ISA-S37.1 *

3530

Calibrator

C REV. E 06/95

D: Air Velocity Transducer, FMA-906V, specs and calibration report

SPECIFICATIONS:

Accuracy: 1.5% FS @ room temperature
2% at 50°C; 3% at 75°C; 3½% at 100°C;
4% at 121°C; add 1% FS below 1000 SFPM
Repeatability: ±0.2% FS
Initial Stabilization Time in Flow: 40 sec
Response Time/After Stabilization:
400 msec to within 63% of final value
at room temperature
Probe: Aluminum oxide ceramic glass
coating, epoxy; probe body 304SS
Probe Temperature:
-40 to 121°C (-40 to 250°F)
Probe Pressure: 150 psig maximum
Electronics Temperature:
Operating: 0 to 50°C (32 to 122°F)
Storage: 0 to 70°C (32 to 158°F)
Operating Relative Humidity: Less
than 80% RH, without condensation
Ambient Temp Compensation: About
5 min for 11°C (20°F) temp change
Outputs: 0 to 5 Vdc or 4 to 20 mA
Voltage Load Resistance:
250 ∧ minimum
Current Loop Resistance:
0 ∧ minute to 400 ∧ maximum; 4-wire
Power: 15 to 24 Vdc, 300 mA
(0 to 100 and 0 to 200 SFPM only);
15 to 18 Vdc, 300 mA (all other ranges)
Accessories: Mating connector prewired
to 4.6 m (15') shielded cable (with
built-in ferrite core) included, standard
Dimensions:
Case: 89 H x 51 W x 31.8 mm D
(3.5 H x 2 W x 1.25" D)
Probe: 6.35 mm (0.25") O.D.,
330 mm (13") length
Short Probe (-S): 6.35 mm (0.25") O.D.,
95 mm (3.75") length
Weight: 160 g (5.6 oz)

Transducer's Calibration Report:

OMEGA ENGINEERING, INC.
An OMEGA Technologies Company

Certificate of Compliance

FMA-906-V   Serial No.: 071119

OMEGA Engineering, Inc. certifies that the instrument referenced above has been fully inspected, tested and calibrated prior to shipment in accordance with the instruction manual supplied. OMEGA further certifies that this instrument meets or exceeds all of the published electrical, mechanical and operational performance characteristics.

All tests and calibrations were performed with instruments, equipment and standards which are traceable to the U.S. National Institute of Standards and Technology.

This instrument has been performance tested at the following test points:

	Standard Test Points	Unit Test Results
1>	0 F.P.M.	0.010 Volts
2>	2000	1.024
3>	5000	2.567
4>	8000	4.015

Accepted By: Tom Hamilton   Date: 11/14/2007

OMEGA Engineering, Inc., One Omega Drive, Box 4047, Stamford, CT 06907-0047
Tel: (203) 359-1660 • FAX: (203) 359-7811
www.omega.com e-mail: info@omega.com

Disk: Forms FN: CertCal
WCS-0594

E: Microphone/Preamplifier Specifications

Model Number
377A12

PRECISION CONDENSER M

Performance	**ENGLISH**	**SI**	
Nominal Microphone Diameter	1/4"	1/4"	
Frequency Response Characteristic	Pressure	Pressure	
Open Circuit Sensitivity (at 250 Hz)	0.25 mV/Pa	0.25 mV/Pa	
Open Circuit Sensitivity (±3 dB) (at 250 Hz)	-72 dB re 1 V/Pa	-72 dB re 1 V/Pa	
Frequency Range (±2 dB)	4 to 20000 Hz	4 to 20000 Hz	
Lower Limiting Frequency (-3 dB)	0.5 to 3 Hz	0.5 to 3 Hz	
Dynamic Range	≤178 dB re 20 μPa	≤178 dB re 20 μPa	[3]
Dynamic Range	>68 dB(A) re 20 μPa	>68 dB(A) re 20 μPa	[4]
Environmental			
Temperature Range (Operating)	-40 to +248 °F	-40 to +120 °C	
Influence of Axial Vibration (0.1g (1 m/s²))	72 dB re 20 μPa	72 dB re 20 μPa	[1]
Electrical			
Capacitance (Polarized)	4.6 pF	4.6 pF	[1]
Polarization Voltage	0 V	0 V	[2]
Physical			
Housing Material	Nickel Alloy	Nickel Alloy	
Venting	Rear	Rear	
Mounting Thread (Preamplifier)	0.2244 - 60 UNS	5.7 mm - 60 UNS	
Mounting Thread (Grid)	0.25 - 60 UNS	6.35 mm - 60 UNS	
Size (Diameter) (with grid)	0.28 in	7.0 mm	
Size (Diameter) (without grid)	0.25 in	6.4 mm	
Size (Height) (with grid)	0.41 in	10.4 mm	
Size (Height) (without grid)	0.36 in	9.1 mm	
Weight	0.06 oz	1.7 gm	[1]

All specifications are at room temperature unless otherwise specified.
In the interest of constant product improvement, we reserve the right to change specifications without notice.
ICP® is a registered trademark of PCB group, Inc.

Model Number 377B01	PRECISION CONDENSER M		
Performance	**ENGLISH**	**SI**	
Nominal Microphone Diameter	1/4"	1/4"	
Frequency Response Characteristic (at 0° incidence)	Free-Field	Free-Field	
Open Circuit Sensitivity (at 250 Hz)	3.16 mV/Pa	3.16 mV/Pa	
Open Circuit Sensitivity (±3 dB) (at 250 Hz)	-50 dB re 1 V/Pa	-50 dB re 1 V/Pa	
Frequency Range (±2 dB)	4 to 80000 Hz	4 to 80000 Hz	
Lower Limiting Frequency (-3 dB)	0.5 to 3 Hz	0.5 to 3 Hz	
Resonant Frequency (90 16 hse Shift)	83 kHz	83 kHz	[1]
Dynamic Range (3% Distortion Limit)	>165 dB re 20 μPa	>165 dB re 20 μPa	
Dynamic Range (Cartridge Thermal Noise)	28 dB(A) re 20 μPa	28 dB(A) re 20 μPa	[1]
Standards Designation (IEC 61094-4)	WS3F	WS3F	
Environmental			
Temperature Range (Operating)	-40 to +248 °F	-40 to +120 °C	
Temperature Coefficient of Sensitivity (14 to 122°F, -10 to 50°C)	0.004 dB/°F	0.009 dB/°C	[1]
Static Pressure Coefficient	-0.007 dB/kPa	-0.007 dB/kPa	[1]
Influence of Humidity (0 to 95%, non-condensing)	<0.1 dB	<0.1 dB	
Influence of Axial Vibration (0.1g (1 m/s²))	60 dB re 20 μPa	60 dB re 20 μPa	[1]
Electrical			
Capacitance (Polarized)	5.1 pF	5.1 pF	[1]
Polarization Voltage	0 V	0 V	[2]
Physical			
Housing Material	Nickel Alloy	Nickel Alloy	
Venting	Side	Side	
Mounting Thread (Preamplifier)	0.2244 - 60 UNS	5.7 mm - 60 UNS	
Mounting Thread (Grid)	0.25 - 60 UNS	6.35 mm - 60 UNS	
Size (Diameter) (with grid)	0.28 in	7.0 mm	
Size (Diameter) (without grid)	0.25 in	6.4 mm	
Size (Height) (with grid)	0.41 in	10.5 mm	
Size (Height) (without grid)	0.35 in	9.0 mm	
Weight	0.06 oz	1.8 gm	[1]

All specifications are at room temperature unless otherwise specified.

In the interest of constant product improvement, we reserve the right to change specifications without notice.

Model Number 377B10	PRECISION CONDENSER M		
Performance	**ENGLISH**	**SI**	
Nominal Microphone Diameter	1/4"	1/4"	
Frequency Response Characteristic	Pressure	Pressure	
Open Circuit Sensitivity (at 250 Hz)	1 mV/Pa	1 mV/Pa	
Open Circuit Sensitivity (±3 dB) (at 250 Hz)	-60 dB re 1 V/Pa	-60 dB re 1 V/Pa	
Frequency Range (±2 dB)	4 to 70000 Hz	4 to 70000 Hz	
Lower Limiting Frequency (-3 dB)	0.5 to 3 Hz	0.5 to 3 Hz	
Resonant Frequency (90°16 hse Shift)	60 kHz	60 kHz	[1]
Dynamic Range (3% Distortion Limit)	>170 dB re 20 µPa	>170 dB re 20 µPa	
Dynamic Range (Cartridge Thermal Noise)	30 dB(A) re 20 µPa	30 dB(A) re 20 µPa	[1]
Standards Designation (IEC 61094-4)	WS3P	WS3P	
Environmental			
Temperature Range (Operating)	-40 to +248 °F	-40 to +120 °C	
Temperature Coefficient of Sensitivity (14 to 122°F, -10 to 50°C)	0.0056 dB/°F	0.01 dB/°C	[1]
Static Pressure Coefficient	-0.004 dB/kPa	-0.004 dB/kPa	[1]
Influence of Axial Vibration (0.1g (1 m/s²))	66 dB re 20 µPa	66 dB re 20 µPa	[1]
Electrical			
Capacitance (Polarized)	5.1 pF	5.1 pF	[1]
Polarization Voltage	0 V	0 V	[2]
Physical			
Housing Material	Nickel Alloy	Nickel Alloy	
Venting	Side	Side	
Mounting Thread (Preamplifier)	0.2244 - 60 UNS	5.7 mm - 60 UNS	
Mounting Thread (Grid)	0.25 - 60 UNS	6.35 mm - 60 UNS	
Size (Diameter) (with grid)	0.28 in	7.0 mm	
Size (Diameter) (without grid)	0.25 in	6.4 mm	
Size (Height) (with grid)	0.41 in	10.4 mm	
Size (Height) (without grid)	0.36 in	9.1 mm	
Weight	0.06 oz	1.8 gm	[1]

All specifications are at room temperature unless otherwise specified.

In the interest of constant product improvement, we reserve the right to change specifications without notice.

ICP® is a registered trademark of PCB group, Inc.

Model Number 426B03	MICROPHONE PREAM		
Performance	**ENGLISH**	**SI**	
Nominal Microphone Diameter	1/4"	1/4"	
Gain	-0.08 dB	-0.08 dB	[1][2]
Frequency Response (±0.1 dB) (re 1 kHz)	5 to 126000 Hz	5 to 126000 Hz	
Frequency Response (±0.2 dB) (re 1 kHz)	3.2 to 126000 Hz	3.2 to 126000 Hz	
Frequency Response (-3 dB) (re 1 kHz)	<0.7 Hz	<0.7 Hz	
Phase Linearity (<1 °)	63 to 20000 Hz	63 to 20000 Hz	
Electrical Noise (A-weight)	<3.2 μV	<3.2 μV	[2]
Electrical Noise (A-weight)	1.9 μV	1.9 μV	[1][2]
Electrical Noise (Flat 20 Hz to 20 kHz)	<5.6 μV	<5.6 μV	[2]
Electrical Noise (Flat 20 Hz to 20 kHz)	3.4 μV	3.4 μV	[1][2]
Distortion (3 V rms input at 1 kHz)	<-70 dB	<-70 dB	
Output Slew Rate	2 V/μS	2 V/μS	[1]
TEDS Compliant	Yes	Yes	[3]
Environmental			
Temperature Range (Operating)	-40 to 158 °F	-40 to 70 °C	
Temperature Range (Storage)	-40 to 185 °F	-40 to 85 °C	
Temperature Response	<0.03 dB	<0.03 dB	
Humidity Range (Non-Condensing)	0 to 95 %RH	0 to 95 %RH	
Humidity Sensitivity	<0.03 dB	<0.03 dB	
Electrical			
Excitation Voltage	20 to 32 VDC	20 to 32 VDC	
Constant Current Excitation	2 to 20 mA	2 to 20 mA	
Impedance (Input)	$2x10^{10}$ ohm	$2x10^{10}$ ohm	[1]
Capacitance (Input)	0.15 pF	0.15 pF	[1]
Output Bias Voltage	10 to 14 VDC	10 to 14 VDC	
Impedance (Output)	<50 ohm	<50 ohm	
Output Voltage (Maximum)	±8 V	±8 V	[1]
Physical			
Housing Material	Stainless Steel	Stainless Steel	
Size (Diameter x Length)	0.25 in x 1.74 in	6.4 mm x 44.2 mm	
Weight	0.21 oz	6 gm	
Electrical Connector	10-32 Coaxial Jack	10-32 Coaxial Jack	
Mounting Thread (Microphone to Preamplifier)	0.2244 - 60 UNS	5.7 mm - 60 UNS	

All specifications are at room temperature unless otherwise specified.
In the interest of constant product improvement, we reserve the right to change specifications without notice.

References:

McKinnis,P. Miller, B. and Ruggles, A, “Interaction Between Main Line Standing Waves and Side Branch Resonance Frequencies.” Fluid Structure Interaction and Moving Boundary Problems IV, WIT Press, 2007. (included below)

J. C. BRUGGEMAN, “Flow Induced Pulsations in Pipe Systems.” PhD Dissertation, Technical University Eindhoven, 1987.

J. C. BRUGGEMAN, A. HIRSCHBERG, M. E. H. van DONGEN, A. P. J. WIJNANDS, and J. GORTER, “Self Sustained Aero-acoustic Pulsations in Gas Transport Systems: Experimantal Study of the Influence of Closed Side Branches.” Journal of Sound and Vibration, Vol. 150, pp. 371-393, 1991.

Interaction Between Main Line Standing Waves and Side Branch Resonance Frequencies

Peter McKinnis, Brett Miller and Arthur Ruggles
WIP Fluid Structure Interaction and Moving Boundary Problems IV, May 2007
University of Tennessee, Department of Nuclear Engineering, Knoxville aruggles@utk.edu

Abstract

Acoustic standing waves may be established in main gas delivery lines that are caused by resonance in branch lines. The branch line resonance frequency is normally determined from the geometry of the branch. Data are presented that show the branch line standing wave couples with the main line standing wave, and a range of side branch resonance frequencies are possible, with multiple frequencies existing in the side branch at the same time in some cases. This phenomenon is important to gas delivery systems where acoustic frequencies and loads must be predicted to facilitate design of the system components.

Keywords: branch line resonance, acoustics, standing waves, fluid-structure interaction.

Introduction

Small branch lines off larger main delivery lines can exhibit acoustic resonance. Branch lines with a reflective obstruction, such as a valve or instrument, are susceptible to a ¼ wavelength standing wave, with a pressure node positioned near where the branch meets the main line, and a pressure anti-node positioned at the obstruction. Of course, higher modes are possible with an odd number of quarter wavelengths existing in the branch such that,

$$f_{natural} = \frac{nc}{4L} \qquad n = 1,3,5,7..... \qquad (1)$$

where c is the sound speed and the characteristic length, L, is the branch length. The branch length is sometimes extended by some fraction of the diameter.

The most common drive for resonance in the branch line is vortex shedding at the branch, where vorticity in the fluid near the wall of the main line becomes free at the branch, and diverts flow periodically into the downstream branch wall, creating periodic pressure perturbations that serve as the energy source for the standing wave in the branch, Rockwell and Naudacher [1]. The frequency of pressure pulses created by the vortex shedding is predicted using the Strouhal number, St=fd/v, with the branch diameter providing the length scale, and v set to the flow velocity in the main line. Coupling between the branch acoustic response and the vortex shedding behaviour allow for a branch to resonate for values for Strouhal number ranging roughly from 0.2 to 0.6, Ziada and Shine, [2]. Strouhal number near 0.4 normally gives the largest amplitude acoustic response in the branch. These values vary with system parameters such as Reynolds number, as examined by Ziada and Buhlmann [3] Bruggeman [4] and Kriesels et al [5].

Some previous applications have motivated enhancements to the basic theory to accommodate system specific attributes. The position of the branch downstream of a fitting such as a valve, orifice or elbow has been shown to influence vortex shedding and the associated Strouhal number response, Ziada and Shine [2], Lamoureau and Weaver [6]. Higher order vortex shedding modes are possible, leading to excitation of acoustic frequencies in branch lines at higher Strouhal numbers, Ziada [7] . Branches positioned across from each other or in tandem may interact to complicate and enhance the acoustic response of the system, Ziada and Buhlmann [3]. Modifications to the geometry of the branch junction to the main line have been explored to mitigate vortex shedding as a coherent source of energy for driving branch line resonance, Weaver and McLeod [8].

While the basic theory provides design guidance associated with the resonance in the branch, the excitation of standing waves in the main line has received little attention. A few studies examine acoustic coupling of branch line modes through the main line, Coffman and Bernstein [9], Ziada and Buhlmann [3], and Ziada and Shine [2]. However, these studies remain concerned with the loading of components in the branch line, such as safety relief valves. Additional knowledge of acoustic loads in the main line is desired for capital intensive applications where more flexibility in design and operation is desired, such as steam supply systems. Components in the steam supply, such as super-heater bundles, steam separator assemblies and steam dryer assemblies may have many structural resonances. Acoustic drives near structural resonance may lead to fatigue failures and commercial performance shortfalls due to loss of equipment availability and reduced component endurance. Avoidance of acoustic excitations corresponding to all or specific structural resonances for conditions of sustained operation is desired. A comprehensive engineering formalism for identifying acoustic oscillations caused by side branches that integrate to cause significant acoustic pressure levels in the main line would be useful for this purpose.

Past efforts have focused on the energy budget of the branch line only, with the vortex shedding mechanism as the energy source, and the energy sinks including damping mechanisms in the branch and acoustic radiation into the main line, Bruggeman [4] and Kriesels et al [5] . In circumstances where damping is low, and outlet paths for the acoustic energy in the main line are limited, the amplitude of the standing wave pattern in the main line can grow quite large, especially if multiple branches are present. Pressure variations in the main line at the branch position influence the acoustic performance of the branch and can modify the branch resonant frequency. This paper explores adjustments to the basic theory to correct for the influence of a standing wave in the main line. The relationship between the standing wave pattern in the main line and the side branch resonance is evaluated through experiment and one dimensional linear acoustic theory. The motivation for the investigation and development is design of nuclear steam supplies, but the modelling outcomes have more general applicability.

The development begins by examining how the main line pressure field may influence the resonant frequency of the branch. The standing wave in the main line is then simulated in the presence of Doppler shift, which modulates the standing wave amplitude with position in the main line. Finally, a low pressure air experiment is presented that provides a simple, easily modified environment to examine the theory.

Wave Forms in Main Lines and How They Interface with Branch Positions

Standing waves of one-quarter wavelength may be induced in closed branch lines as represented in eq. 1 for the primary mode with n equal unity. The model assumes that the ratio of the diameter of the branch line over the diameter of the main line is small, such that the pressure at the branch line entrance is near zero. In the case where standing pressure waves build in the main line, the pressure at the inlet of the branch line is equal to the pressure in the main line at the location of the branch. Fig.1 shows the relationship between pressure oscillations in the main line on the wavelength of the standing wave in the branch line.

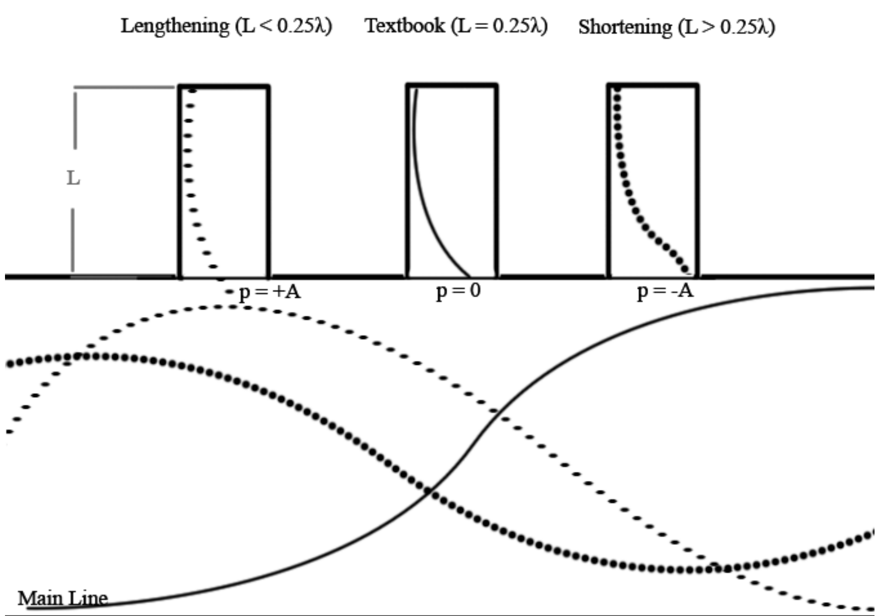

Lengthening and shortening of standing waves when subjected to pressure oscillations in the main line.

From fig. 1, the length of the branch line equal to one-quarter of the primary mode wavelength holds true when the branch line is located over a pressure node in the main line. However, as the acoustic pressure in the main line moves towards an antinode, the wavelength of the standing wave in the branch either increases – moving out into the main line and remaining in phase with the pressure variation in the main line, or decreases – moving into the branch line and operating out of phase with the main line pressure response.

Because of this phenomenon, the natural frequency of the branch line is expected to shift depending on its location relative to the standing wave pattern in the main line. If a term, β, is defined as,

$$\beta = L - \frac{1}{4}\lambda \qquad (2)$$

then standing waves are induced in the branch line when the natural frequency corresponds to the length of the branch line in the following way:

$$f_{natural} = \frac{nc}{4(L-\beta)} \quad n = 1,3,5,7..... \qquad (3)$$

This is a manipulation of eq. 1. For the fundamental mode, the value of β can be determined from the pressures at the inlet and top of the branch line using the following:

$$\beta = \frac{2\theta L}{2\theta + \pi} \qquad (4)$$

where θ is defined as,

$$\theta = \sin^{-1}\left(\frac{P_{inlet}}{P_{\max}}\right) \qquad (5)$$

P_{inlet} is the pressure at the inlet of the branch line and P_{max} is the pressure at the top of the branch line.

Examination of the Doppler Effect in the Main Line

The branch line is not stationary with respect to the steam flow. Therefore, the pressure wave caused by the branch in the main line is shifted in wavelength because of the Doppler effect. Upstream of the branch line, the wavelength is shorter, and downstream of the branch line, the wavelength is longer. Note that in this application, from the perspective of a stationary observer (i.e., instrumentation, branch position or Eulerian reference), the wavelength is shifted, not the frequency. The Doppler shift in wavelength can be written as a function of Mach number:

$$\lambda_{ds} = \lambda(1+M) \qquad (6)$$

$$\lambda_{us} = \lambda(1-M) \qquad (7)$$

Where λ_{ds} is the shifted wavelength downstream of the branch line, λ_{us} is the Doppler shifted wavelength upstream from the branch line, λ is the unshifted wavelength, and M is the Mach number. Thus the normalized pressure wave can be written as a simple sine function.

$$P_{us} = \sin\left(\frac{2\pi x}{\lambda_{us}}\right) \qquad (8)$$

$$P_{ds} = \sin(\frac{2\pi x}{\lambda_{ds}}), \qquad (9)$$

The sum of the upstream and downstream travelling waves causes a composite wave form inside of the main line. An example of this type of waveform is shown in fig. 2 with the left boundary corresponding to a compliant interface. If the branch were positioned near 60 meters for the example system in fig. 2, then one would expect some shift in branch resonance frequency, or perhaps two distinct frequencies may be observed in the branch as discussed in section 2 of this paper.

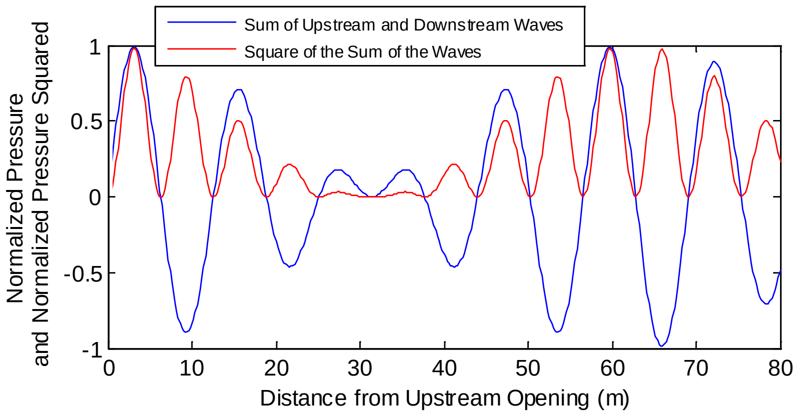

Interaction of Upstream and Down Stream Doppler Shifted Waveforms

Experimental

The application of interest in this effort is a steam supply with several branch lines and other flow management hardware such as valves and fittings. Early examination of acoustic pressures at discrete locations on the main steam lines exposed very complex behaviour. A simple, atmospheric pressure, air test facility was developed to examine basic attributes of the relationship between standing waves in the main line and the branch line.

Experimental Facility

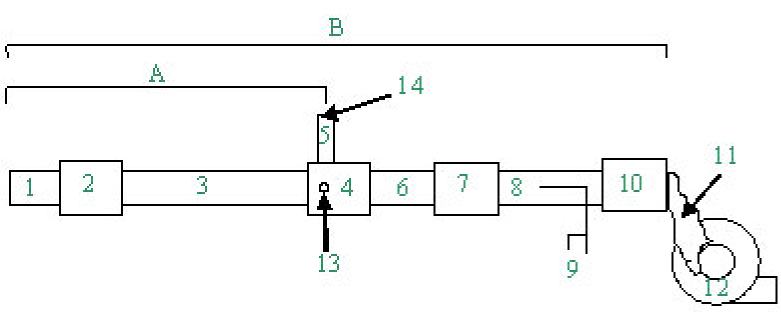

Diagram of Experimental Apparatus.

The experimental setup shown in fig. 3 consists of a main line 297 cm long made of sections of 7.6 cm (3 in) diameter PVC piping connected to a blower via flexible aluminium tubing. Air was drawn through the apparatus from section 1 as labelled in fig. 3, toward the Dayton™ model 3N669A 3.7 kW blower, section 12. Velocities up to 43 m/s are possible. Sections 1, 3, 6, and 8 are 7.6 cm diameter Schedule 40 PVC piping. These sections were interchangeable so as to vary the relative position of the branch line with respect to the upstream and downstream boundary. The upstream boundary, positioned left of section 1, was open to the room and contained no obstructions for several diameters in every direction. The downstream boundary was a transition from PVC piping (section 10) to flexible corrugated aluminium tubing (section 11). Sections 2,4,7, and 10 represent couplings. Section 5 represents a short capped branch line made of 1.9 cm (3/4 in) PVC pipe. The branch was carefully prepared by drilling a hole through the pipe and solvent welding the branch on top of the hole. This yielded a sharp branch edge as shown in fig. 4.

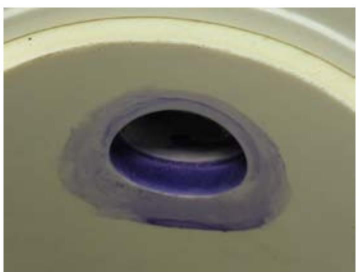

A View from the inside of the pipe of the sharp branch edge.

The apparatus contains 2 through wall mounted PCB Piezotronics™ model 130D20 microphones, located at positions 13 and 14 in fig. 3, and another identical microphone on a measuring tape that could be moved in the main line. A pitot tube was used to measure fluid velocity and is shown at position 9. It was connected to an Omega™ model PX653-05D5V electrical differential pressure cell that had a response time of 250 ms. The microphone was positioned so that the diaphragm was located in the stream just below the branch line. It was sampled at 100 kS/s with a National Instruments DAQ model NI USB-9162.

Matrix for Data Acquisition

The behaviour of the system can be complex, and it is desired to characterize the system performance thoroughly. Two initial permutations of the facility geometry were planned and are reported here, both conducted at a constant main line flow velocity of 38 m/s, corresponding to a flow Mach number of 0.112.

Experiment 1 - Constant Length

The position of the branch line, section 5, was varied by changing the length of pipes 1 and 6. They were changed such that the total length from the front edge of pipe 1 to the back edge of coupling 10 (Length B) remained constant at 297 cm. Ten experiments were done such that the distance from the upstream boundary to the centre of the branch line was varied from 199 cm to 222 cm in 2.54 cm increments. For each setup, the stream velocity and pressure were measured in two-second packets. The pressure was sampled at 100 kS/s. Twenty such data packets were measured and analyzed for each experimental setup.

Experiment 2 – Variable Length

The position of the branch line was varied relative to the upstream boundary by changing the length of pipe 1 (Length A). However, the position of the branch relative to the downstream boundary remained constant, causing a change in the total length of the pipe (Length B). Once again, ten pipe configurations were explored. In each successive setup, the length of pipe 1 was lengthened by 2.54 cm, causing the distance from the upstream boundary to vary from 199 to 222 cm. The distance from the pipe to the downstream boundary was held constant at 58.4 cm. Once again twenty, two-second, data packets were obtained for each piping configuration and the pressure was sampled at 100 kS/s.

Data Reduction and Calculations

The branch line used for reported data was 16.0 cm long. Therefore, with sound speed equal to 340 m/s the expected frequency is 531 Hz. The pressure data is processed in two-second time series packets. A Hanning window is applied to each packet and a Fourier transform performed using Matlab™. The peaks near 531 Hz were examined manually.

Results

The time series pressure data from the microphone positions are treated in the frequency domain. Two second time series are used throughout this evaluation, but other time series lengths were examined before selecting this time window as an appropriate and representative value.

Experiment 1

In experiment 1, the waveform produced by the branch line had a great deal of variance. Six of the ten configurations showed a single frequency peak near the expected value. Fig. 5 shows the power density spectra typical of all six of these configurations. The frequency varied slightly in these experiments from 511 to 516 Hz.

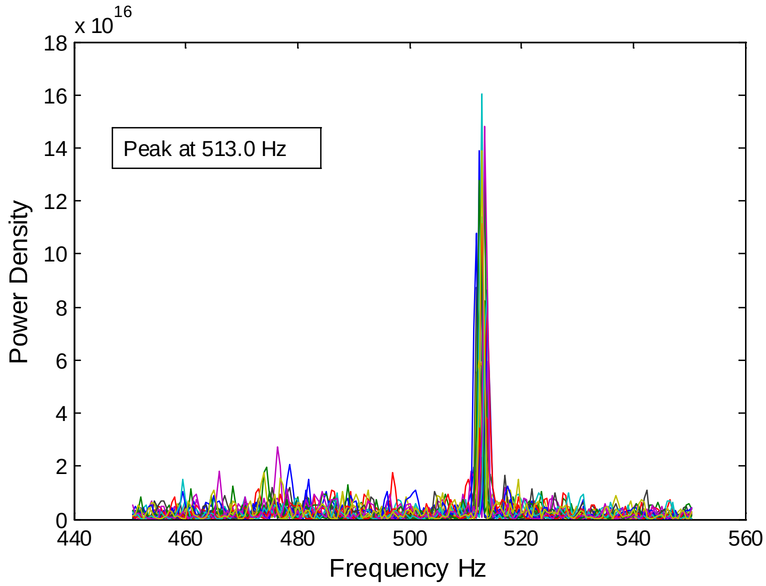

Typical Single Peaked Power Spectra with Peak Near the Expected Value – All 20 Data Packets Graphed Individually

Four of the ten configurations showed two significant frequency peaks. Fig. 6 shows spectra typical of these configurations. From fig. 6, it may seem that all twenty of the data packets for the given configuration express both peaks. However, some do not express the smaller high frequency peak as can be seen in fig. 7b. Additionally, some data packets express a low frequency peak that is smaller than the high frequency peak, as shown in fig. 7c. The waveform shifts in expression between the low and high frequency peak over relatively long time periods.

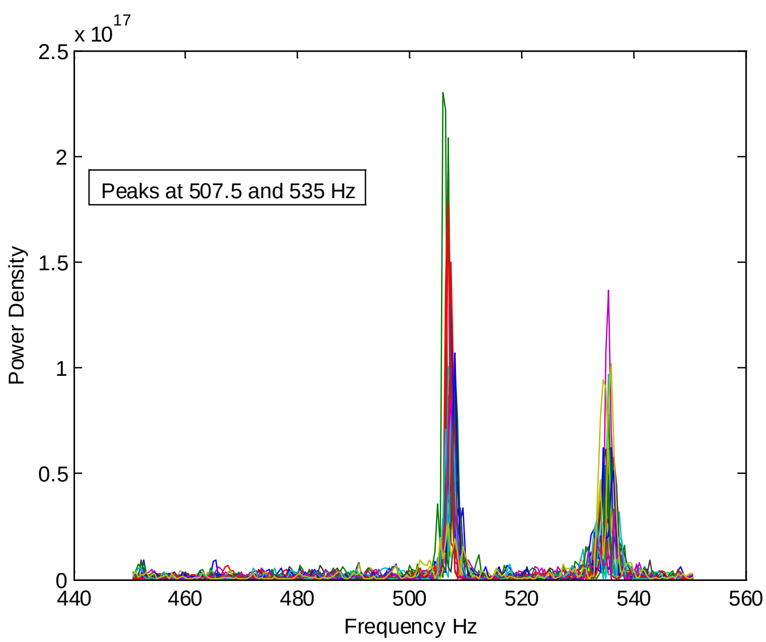

Typical 2 Peaked Power Spectra – 20 Data Packets Graphed Individually

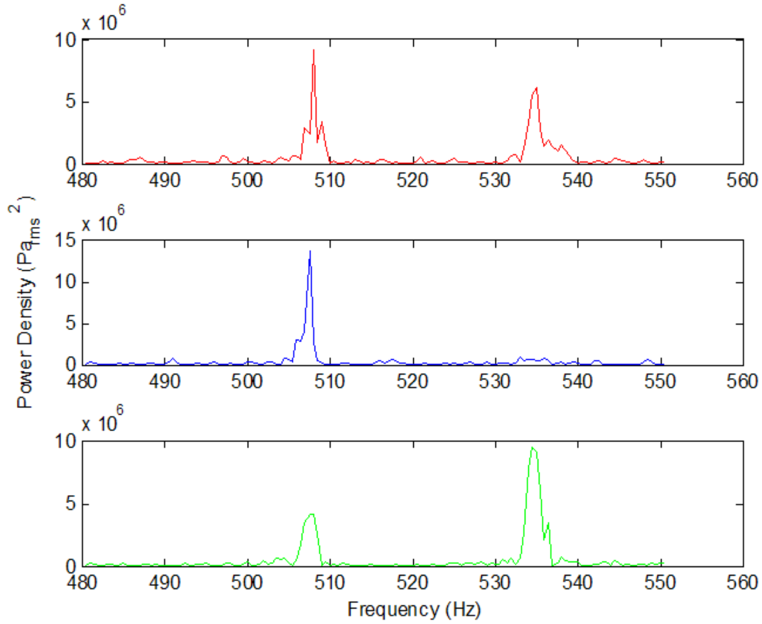

Shifting of Branch Energy Between multiple peaks in time. 7a (top) Peaks are typical of time averaged values. 7b (Middle) only the low frequency peak is expressed. 7c (bottom) the high frequency peak has a greater amplitude

Experiment 2

In this experiment, with the position of the branch relative to the downstream end of the main line fixed, all configurations had stable, high-amplitude peaks, with fig. 8 showing typical power spectra. As the branch line position was varied, the branch frequency, and the frequency in the main line, varied over 5.5%. This variance is a near-linear function of the main line length as shown in fig. 9. Note that between 215 cm and 217 cm the frequency promptly increases before beginning to decrease again.

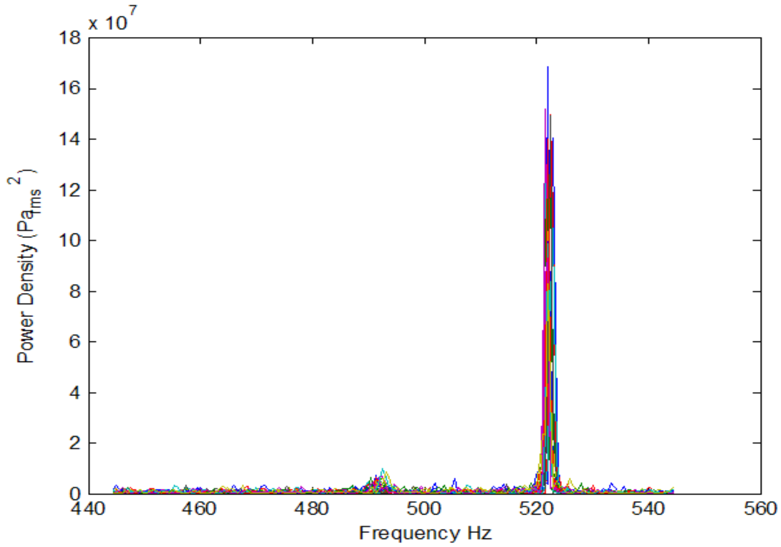

Branch Power Density with Branch 215 cm from upstream boundary – 20 Data Packets Graphed Individually

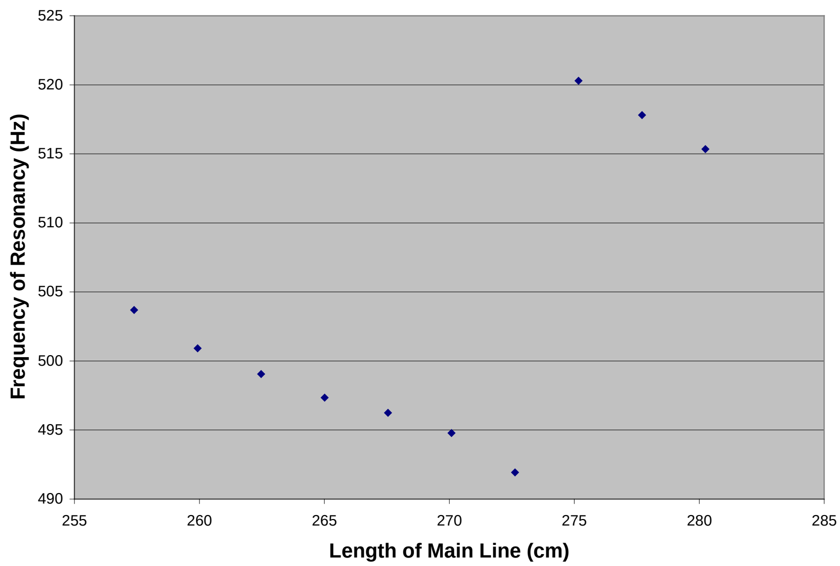

Frequency Shift Due to Variation of Main Pipe Length

The frequency content of the pressure at the end of the branch closely corresponds to the behaviour of the pressure at the base of the branch for all the geometries evaluated.

Interpretation of Results

The main line has compliant boundary conditions at each end, and therefore has resonant frequencies corresponding to situations where an integer number of half wavelengths exist in the line,

$$f = \frac{cn}{2L_m} \qquad n = 1,2,3,.... \qquad (10)$$

The drive frequency from the branch supplies energy to the resonant frequency in the main line that closely matches the branch resonance frequency. Variation in the main line length varies the main line resonance frequency, as shown clearly in fig. 9. The frequency jumps to change the number of half wavelengths in the main line when the main line resonance departs too far from the preferred branch drive frequency. The transition depicted in fig. 9 near main line length of 274 cm corresponds to a transition from n equal nine to n equal ten in eq. 10. The branch drive frequency and the main line resonance lock-in, with both the branch reflective end pressure, and main line pressure exhibiting the same primary frequency content. The wavelength in the branch line and the wavelength in the main line move from their preferred independent values to create a single resonance frequency for the system.

In the first experiment, where the branch position is varied in a main line of fixed length, there are branch locations where two primary resonance frequencies exist in the main line. The branch appears to be conflicted about which frequency to prefer, wandering relatively slowly between two distinct values. More investigation is planned to better characterize and understand this behaviour.

Conclusions

Side branch resonance frequencies couple with main line resonance frequencies, allowing a branch to resonate over a range of frequencies as the length of the main line is altered. This is important to engineering applications where the resonant frequency of a branch must be predicted with some accuracy. Current engineering practice does not include consideration of the standing wave patterns in the main line when branch line resonance is evaluated. This can lead to significant errors when conditions are favourable for a standing wave pattern to build in the main line.

The acoustic energy balance for the branch and main line together includes a source term associated with vortex shedding at the branch, and damping mechanisms and acoustic radiation from the main line ends. Wave amplitudes will build in the branch and main line when damping and radiation terms are small relative to the source terms, until a steady state energy balance is achieved. The steady state pressure amplitudes tend to increase as the system pressure or gas density is increased due to the behaviour of the source term relative to the damping and radiation terms, Buggeman [4] and Kriesels et al, [5]. This implies the frequency coupling observed in the low pressure air facility may be more pronounced in higher pressure situations.

The pressure amplitudes in the main line of this experiment are too low relative to the branch line pressures to allow examination of branch frequency shifting that may occur due to pressure variation in the main line, as proposed in section 2 of this paper. However, significant wavelength and associated frequency accommodation appears to be possible in the branch line and main line to allow lock-in of a single, system-wide, resonance frequency. The branch line resonance frequency is coupled to the resonance frequency of the main line, and follows the resonance frequency of the main line as the main line length is varied. The branch resonance frequency varied over a six percent range in this experiment. However, larger ranges are likely for other configurations of branch line length and main line length. The coupling may also be more pronounced in high pressure systems, allowing branch resonance frequencies to vary over larger spans. This has important implications when resonant frequencies are being evaluated for use in predicting structural loadings in design of large systems.

References

[1] Rockwell, D. and Naudascher, E., “Review-Self Sustaining Oscillations of Flow Past Cavities.” Journal of Fluids Engineering, Vol. 100, 152-165, 1978.

[2] Ziada, S. and Shine, S., “Strouhal Numbers of Flow-Excited Acoustic Resonance of Closed Side Branches.” Journal of Fluids and Structures, Vol. 13, 127-142, 1999.

[3] Ziada, S. and Buhlmann, E. T., “Multiple Side-Branches as Tone Generators.” Proceedings of International Mechanical Engineering Conference, paper 0416/009, pp. 435-444, 1991.

[4] Bruggeman, J. C., “Flow Induced Pulsations in Pipe Systems.” PhD Thesis, Technische Universiteit Eindhoven, 1987.

[5] Kriesels, P. C., Peters, M. C. A. M., Hirschberg, A., Wijnands, A. P. J., Iafrati, A., Riccardi, G., Piva, R., Bruggeman, J. C., “High Amplitude Vortex Induced Pulsations in Gas Transport Systems.” Journal of Sound and Vibration, Vol. 184, 343-368, 1995.

[6] Lamoureux, P. N. and Weaver, D. S., “The Effects of Turbulence and Damping on Pipeline Acoustic Resonance.” Proceedings of the Institution of Mechanical Engineers, Flow Induced Vibrations, paper C416/093, May 20-22, 1991.

[7] Ziada, S., “A Flow Visualization Study of Flow-Acoustic Coupling at the mouth of a Resonant Side Branch.” Journal of Fluids and Structures, Vol. 8, 391-416, 1994.

[8] Weaver, D. S., and MacLeod, G. O., “Entrance Port Rounding Effects on Acoustic Resonance in Safety Relief Valves.” Pressure Vessels and Piping, Vol 389, Flow-Induced Vibration, 291-296, 1999.

[9] Coffman, J. T. and Bernstein, M. D., “ Failure of Safety Valves Due to Flow Induced Vibration.” Journal of Pressure Vessel Technology, Vol. 102, 112-118, 1980.